ACADEMIC PRESS

Available online at www.sciencedirect.com
SCIENCE DIRECT®

NeuroImage

NeuroImage 18 (2003) 895–907

www.elsevier.com/locate/ynimg

A comprehensive study of gray matter loss in patients with Alzheimer's disease using optimized voxel-based morphometry

G.B. Karas,[a,b,c,*] E.J. Burton,[d] S.A.R.B. Rombouts,[c,e] R.A. van Schijndel,[e] J.T. O'Brien,[d] Ph. Scheltens,[c,f] I.G. McKeith,[d] D. Williams,[d] C. Ballard,[d] and F. Barkhof[a,b,c]

[a] *Department of Diagnostic Radiology, Vrije Universiteit Medical Center, Amsterdam, The Netherlands*
[b] *Image Analysis Center, Vrije Universiteit Medical Center, Amsterdam, The Netherlands*
[c] *Alzheimer Center, Vrije Universiteit Medical Center, Amsterdam, The Netherlands*
[d] *Institute for Ageing and Health, University of Newcastle upon Tyne, Newcastle upon Tyne, UK*
[e] *Department of Clinical Physics and Informatics, Vrije Universiteit Medical Center, Amsterdam, The Netherlands*
[f] *Department of Clinical Neurology, Vrije Universiteit Medical Center, Amsterdam, The Netherlands*

Received 3 June 2002; revised 28 October 2002; accepted 26 November 2002

Abstract

Voxel-based morphometry (VBM) has already been applied to MRI scans of patients with Alzheimer's disease (AD). The results of these studies demonstrated atrophy of the hippocampus, temporal pole, and insula, but did not describe any global brain changes or atrophy of deep cerebral structures. We propose an optimized VBM method, which accounts for these shortcomings. Additional processing steps are incorporated in the method, to ensure that the whole spectrum of brain atrophy is visualized. A local group template was created to avoid registration bias, morphological opening was performed to eliminate cerebrospinal fluid voxel misclassifications, and volume preserving modulation was used to correct for local volume changes. Group differences were assessed and thresholded at $P < 0.05$ (corrected). Our results confirm earlier findings, but additionally we demonstrate global cortical atrophy with sparing of the sensorimotor cortex, occipital poles, and cerebellum. Moreover, we show atrophy of the caudate head nuclei and medial thalami. Our findings are in full agreement with the established neuropathological descriptions, offering a comprehensive view of atrophy patterns in AD.

Introduction

Alzheimer's disease (AD) will become one of the major public health problems for the Western World in the coming decades. Aging of the population will lead to more and more people developing AD. In the long run, caring for AD patients will be a major financial backlash for the health care system (Gutterman et al., 1999; Trabucchi, 1999). In order to provide care for these patients though, it is important to diagnose this disease and differentiate it from other dementia subtypes.

Medial temporal lobe (MTL) atrophy, as seen on MRI scans of AD patients, is a sensitive marker of AD, even in mild forms of the disease (de Leon et al., 1993; Fox et al., 1996; Scheltens et al., 1992). There are various ways to estimate brain atrophy on MRI. Visual inspection for the presence of atrophy (Scheltens et al., 1997) may be adequate in a routine clinical setting, but is not enough when quantitative measures are needed, for example, to estimate rate of tissue loss during a clinical trial. To assess such changes in a single brain structure, the region-of-interest (ROI) analysis technique may be employed (Pruessner et al., 2000), in which an experienced operator outlines the structure in question in a series of contiguous sections on a computer screen. ROI analysis constitutes, up to now, the gold standard in brain atrophy measurements (Jack et al., 1992), but there are major shortcomings such as observer/operator dependency and bias in brain structure and anatomical region boundary selection (Pruessner et al., 2000). In order to overcome these shortcomings, automated tech-

* Corresponding author. PO Box 7057, 1007 MB, Amsterdam, The Netherlands. Fax: +31-20-4041945.
E-mail address: GB.Karas@vumc.nl (G.B. Karas).

1053-8119/03/$ – see front matter © 2003 Elsevier Science (USA). All rights reserved.
doi:10.1016/S1053-8119(03)00041-7

niques have been developed (Freeborough and Fox, 1997, 1998; Frisoni et al., 1996; Smith et al., 2001; Thompson et al., 2000), the goal of which is to automatically analyze whole-brain structural MRI scans, avoiding a priori selection of regions and eliminating observer variability.

Voxel-based morphometry (VBM) is one such method developed for automated unbiased analysis of structural MRI scans. It has been used in a variety of settings and diseases (Ashburner and Friston, 2000), including VBM analysis of brain tissue loss in AD (Baron et al., 2001; Rombouts et al., 2000). However, the initial implementation of VBM has led to debate about the limitations of affine and low-order registration algorithms (Ashburner and Friston, 2001; Bookstein, 2001). It has been argued that imperfect registration of MRI scans to a common template can lead to false estimates of atrophy (Bookstein, 2001). Moreover, tissue classification errors during automated segmentation of brain tissue classes will produce an artificial thin rim of periventricular gray matter. In the current analysis, we tackled these two issues and applied dementia-specific VBM to study patterns of atrophy in AD compared to elderly controls, attempting to visualize similar atrophy patterns on the MRI analysis to the ones described neuropathologically (Braak et al., 1999; Braak and Braak, 1991).

Materials and methods

Subjects

Twenty-five patients with AD and twenty-five healthy controls of comparable age, recruited among spouses and friends of the patients, were included in the study. Written informed consent was obtained for all subjects. Approval of performance of MRI scans by local ethics committee was granted. All dementia subjects underwent a neuropsychological test battery. Cognitive function was measured using the Cambridge Mental Disorders of the Elderly Examination (CAMCOG) (Roth et al., 1986), which incorporated the Mini-Mental State Examination (MMSE)(Folstein et al., 1975). For controls, the cutoff for MMSE was set to greater than or equal to 24, but none of the controls had a MMSE score lower than 25.

Depressive symptoms were also rated using the Montgomery Asberg Depression Rating Scale (MADRS) (Montgomery, 1979), in order to exclude major depression. Control subjects underwent detailed examination to exclude evidence of dementia (from history or CAMCOG score <80), depression (from history or score >10 on MADRS), and neurologic, physical, and psychiatric disorders before being recruited into the study.

The diagnosis of AD was made by a consensus of three experienced raters following the consensus criteria of the National Institute of Neurological and Communicative Disorders and Stroke and Alzheimer's Disease and Related Disorders Task Force (NINCDS/ADRDA) AD (McKhann et al., 1984). Baseline characteristics of the group are given in Table 1, showing that the group consists of mild–moderate late onset AD patients.

Table 1
Baseline characteristics of AD and Control groups

	Age years (SD)[a]	Disease duration months (SD)	MMSE score (SD)[b]
AD	77.3 (4.9)	43.5 (26)	15.6 (5.2)
Controls	76.1 (4.7)	—	28.1 (1.5)

[a] Ages were comparable at $P = 0.2$.
[b] MMSE scores were statistically significant at $P < 0.0001$.

Magnetic resonance imaging was performed on a 1.0-T Siemens Magnetom Impact Expert MRI system (Siemens, Erlangen, Germany). Whole brain T1-weighted 3D MPRAGE (magnetization-prepared rapid-acquisition gradient echo) data sets were acquired in the sagittal plane (TR, 11.4 ms; TE, 4.4 ms; TI, 400 ms; 256×256 matrix; 1-mm slice thickness; flip angle, 15°). Voxel sizes were $1 \times 1 \times 1$ mm (isotropic voxels). The same radiographer and standard head positioning were used throughout.

Image processing

Data analysis was performed on a SUN SPARC Ultra 10 workstation (Sun Microsystems, Mountain View Inc., CA, USA), using mainly statistical parametric mapping software (SPM99, Wellcome Department of Cognitive Neurology, Institute of Neurology, London, UK, http://www.fil.ion.ucl.ac.uk/spm/) (Friston et al., 1995) in conjunction with MATLAB version 6 (The Mathworks, Inc., MA, USA). Display of 3D images and image blending for display was done with IDL version 5.5 (Interactive Data Language, Research Systems Inc., Boulder, CO). In-house developed software in the C language and IDL was used to solve or automate certain processing problems.

Original VBM

The dementia-specific method we propose (Fig. 1) has taken into account previous VBM studies applied on dementia (Baron et al., 2001; Rombouts et al., 2000) and recent approaches of creating local templates (Good et al., 2001b, 2001a; Thompson et al., 2001).

Prior to image preprocessing a single investigator checked the images for artifacts and manually reorientated them using SPM99 so that they were centred on the anterior commissure (Good et al., 2001b). The image data sets were then subjected to the following automated image processing steps prior to statistical analysis.

In the original VBM method applied in dementia, volumes are first registered to a standard brain template. Registration of volumes to a common target is referred to as

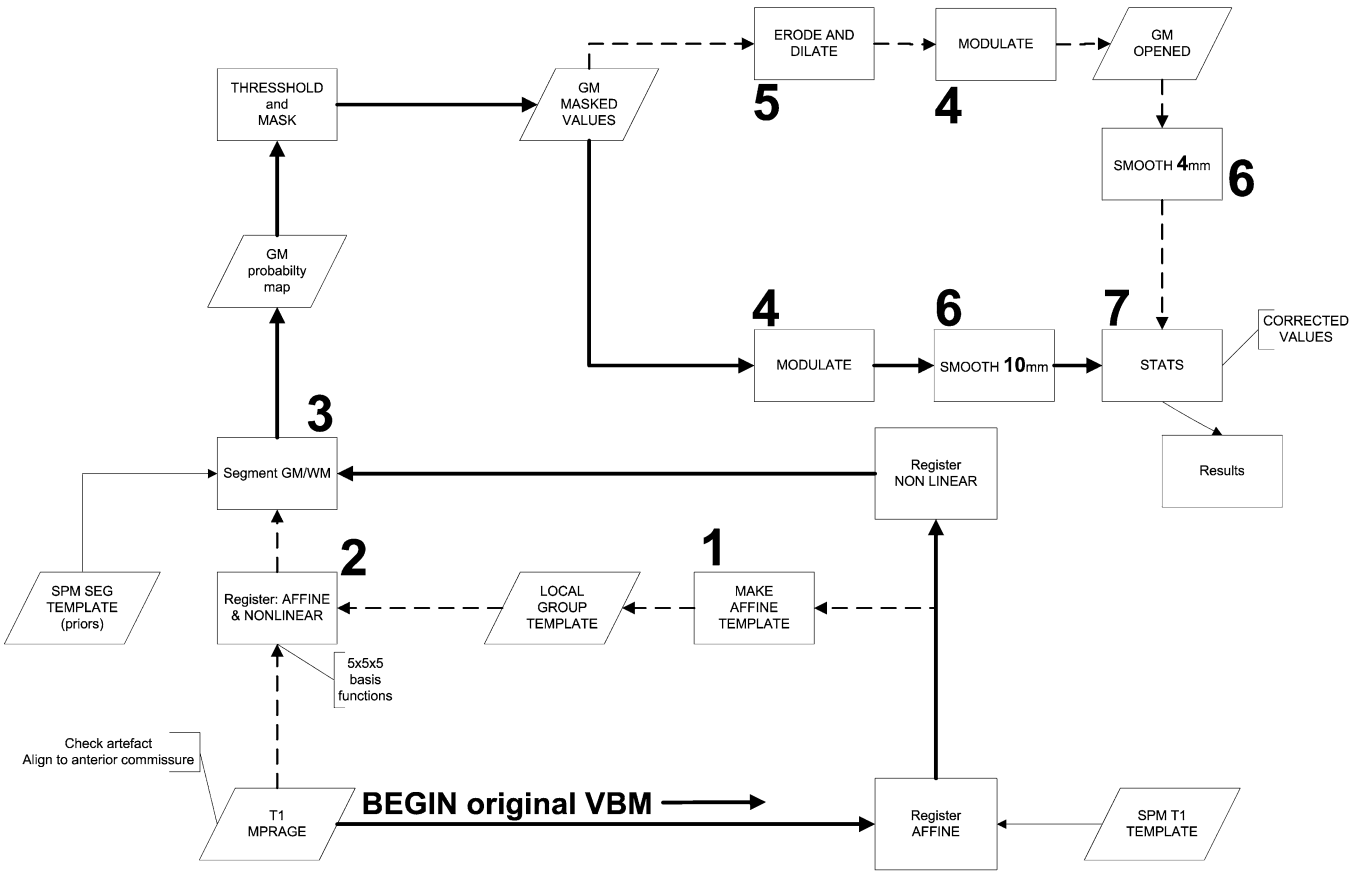

Fig. 1. VBM protocol applied in dementia. We began by performing an original VBM in order to create the local template (step 1). Subsequently we followed the proposed steps (2 to 7). Numbers in bold reflect the VBM steps described in the under Materials and Methods. Notice that we reached the statistics box by either opening the volume or not, depending on whether we wished to analyze deep structures or cortical regions.

normalization. The target is usually a template of the same modality (Rombouts et al., 2000). In the first VBM studies of tissue loss in AD, the template used was the default of SPM99, which was created by averaging the structural MRI scans of 152 healthy young controls. Subsequently, a Bayesian segmentation of gray/white matter and cerebrospinal fluid partitions is performed and eventually smoothing and statistical analysis. Variations do exist, for example, segmented gray matter maps may be registered to standard space once more and then subjected to statistical analysis (Baron et al., 2001). The essential problem with the original VBM applied to brains with atrophy is that MRI scans of AD patients have a different geometry than those of controls (mainly ventricular enlargement and displacement of structures). As a result, controls will match the standard template better than AD patients; especially near strong intensity gradients, one runs the danger of measuring structure displacement on top of atrophy (Bookstein, 2001); hence the need for a study-specific template.

Optimized VBM

Study-specific template formation

We attempted to tackle the problem of registration to standard space by creating a study-specific local group template. Local refers to a template created by averaging the scans of the patients and controls in the current data set together in one template. Image volumes were first roughly normalized to standard space by using a 12-parameter affine model without any nonlinear factors. Spatial normalization uses a 12-parameter affine transformation to match each image volume to the template image volume by minimizing the residual sum of squared differences between the image and the template (Ashburner and Friston, 1997). The standard space model used was the 152 average T1 MNI (Montreal Neurological Institute) template. Subsequently the transformed scans were averaged (Fig. 2). We decided not to perform iterative averaging of transformation matrices for this study (by using matrix logarithms and exponents), since our goal was to search for local group differences and not create a state-of-the-art disease probability atlas (Toga and Thompson, 2001; Woods et al., 1998). It should be noted that the template was created with input from both the patients and controls. In a last step, the created average volume was smoothed with a Gaussian of 8 mm full-width at half-maximum (FWHM). Nonlinear components were not used for template creation in order to

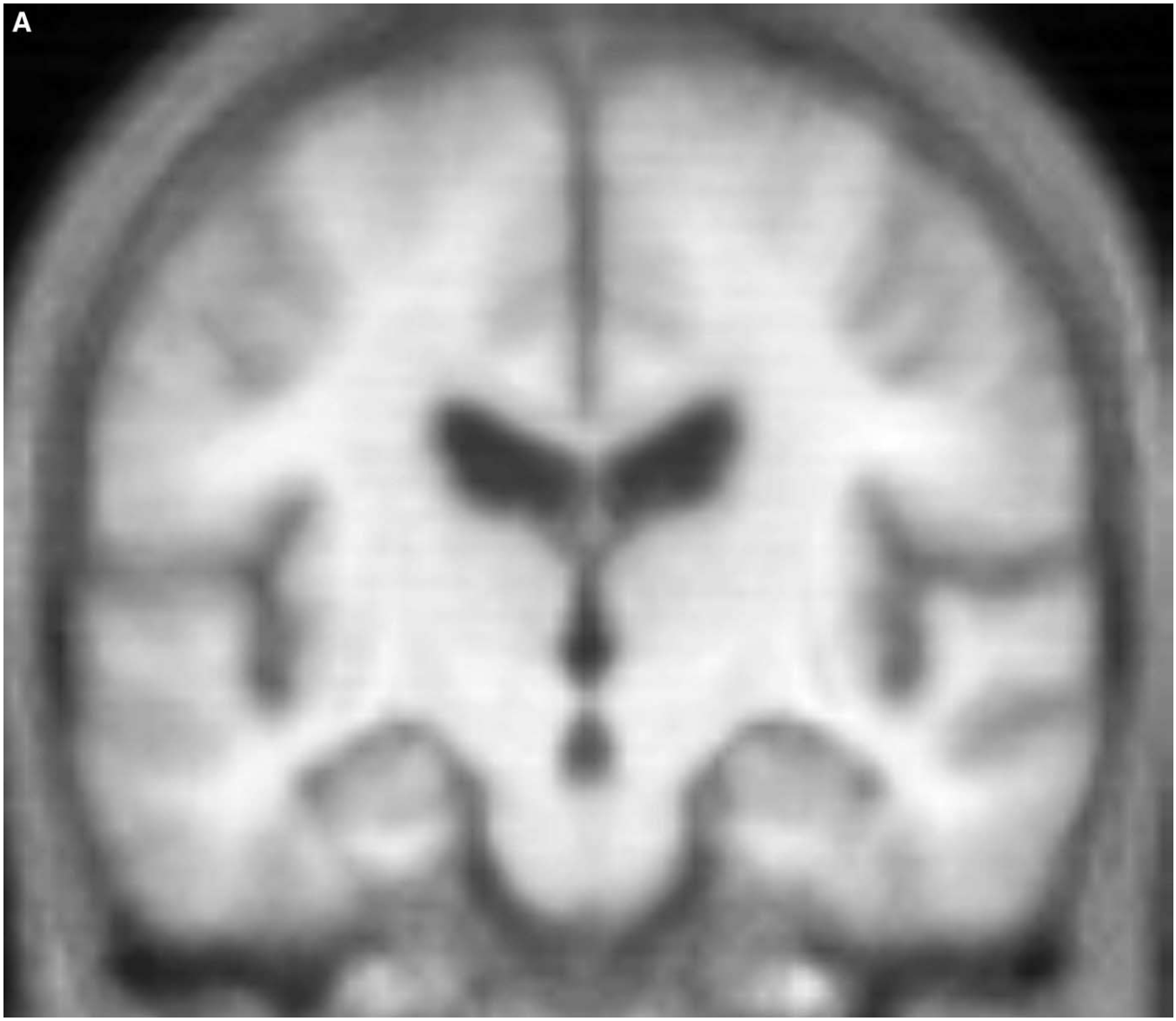

Fig. 2. Local group templates versus standard space template. (A) A local group affine template created by averaging both controls and AD patients; (B) the same template smoothed with a kernel of 8 mm; and (C) the original SPM template. Since the scans we used for template creation were already registered to standard space, the group-specific template also matches standard space. We notice, however, that our template already demonstrates a mixture of aging- and AD-related changes: enlarged lateral ventricles and third ventricle, widened Sylvian fissure, and atrophic hippocampi bilaterally. Because of smoothing it is hard to tell the degree of cortical atrophy only by visual inspection.

preserve group affine geometry (Toga and Thompson, 2001; Woods et al., 1998).

Scan to template matching

This was achieved by affine registration of each scan to the aforementioned local group template and subsequently performing nonlinear iterations using $5 \times 5 \times 5$ basis functions to account for global nonlinear shape differences (Ashburner and Friston, 1999). Normalization ends with the resampling of the transformed volumes by trilinear interpolation to a voxel size of $1 \times 1 \times 1$ mm. By registering to the local group template rather than a standard template, systematic registration bias for any particular group is reduced.

Segmentation

After normalization, the images were automatically segmented using a cluster analysis technique to identify voxels belonging to particular tissue types. This process, based on prior probability maps about the relative distribution of tissue types, partitions brain into gray matter (GM), white matter (WM), cerebrospinal fluid (CSF), and a fourth partition comprising skull, fat, muscle, and other unclassified voxels (Ashburner and Friston, 2000).

Volume preserving modulation

Although affine normalization does change the global volumes to bring them into template space and facilitate

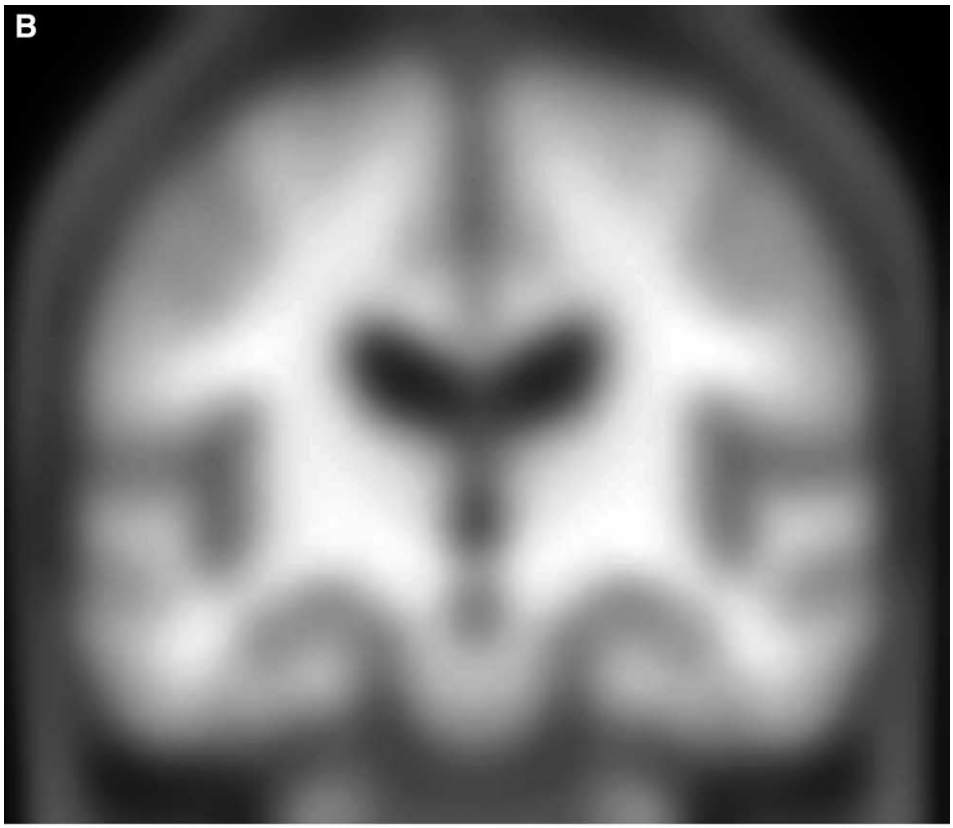

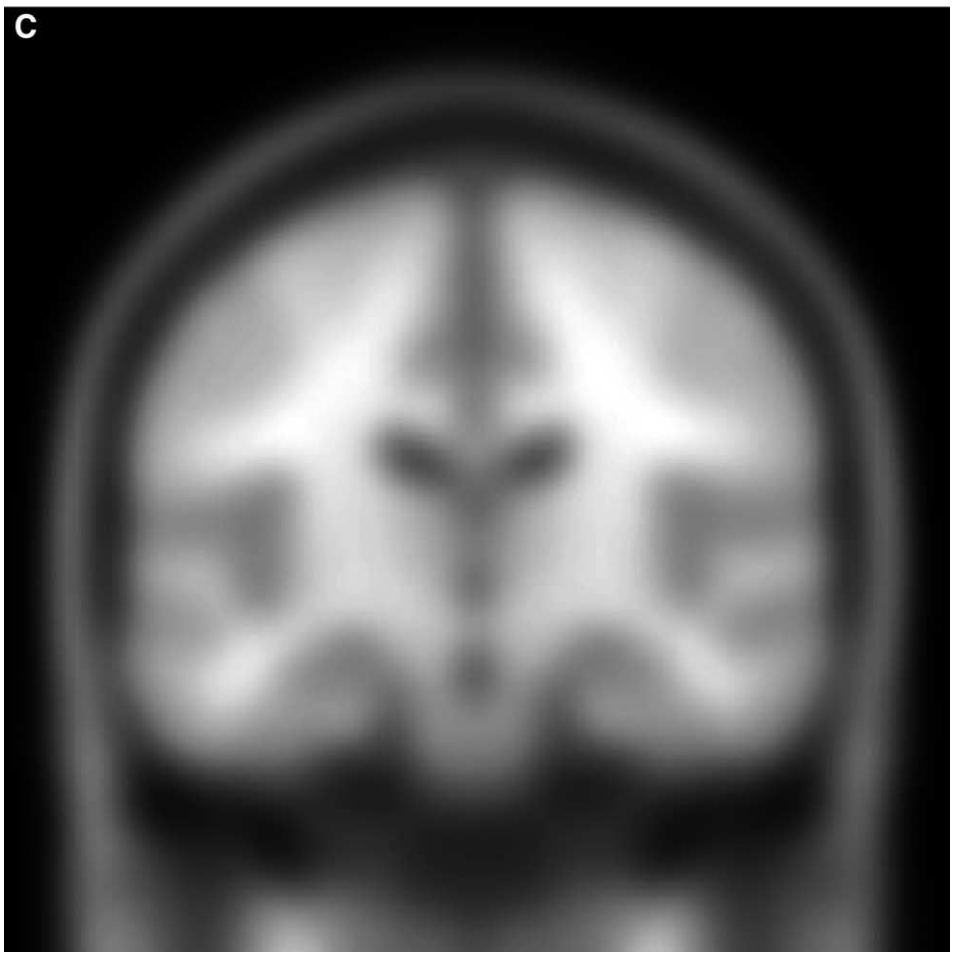

Fig. 2 (*continued*)

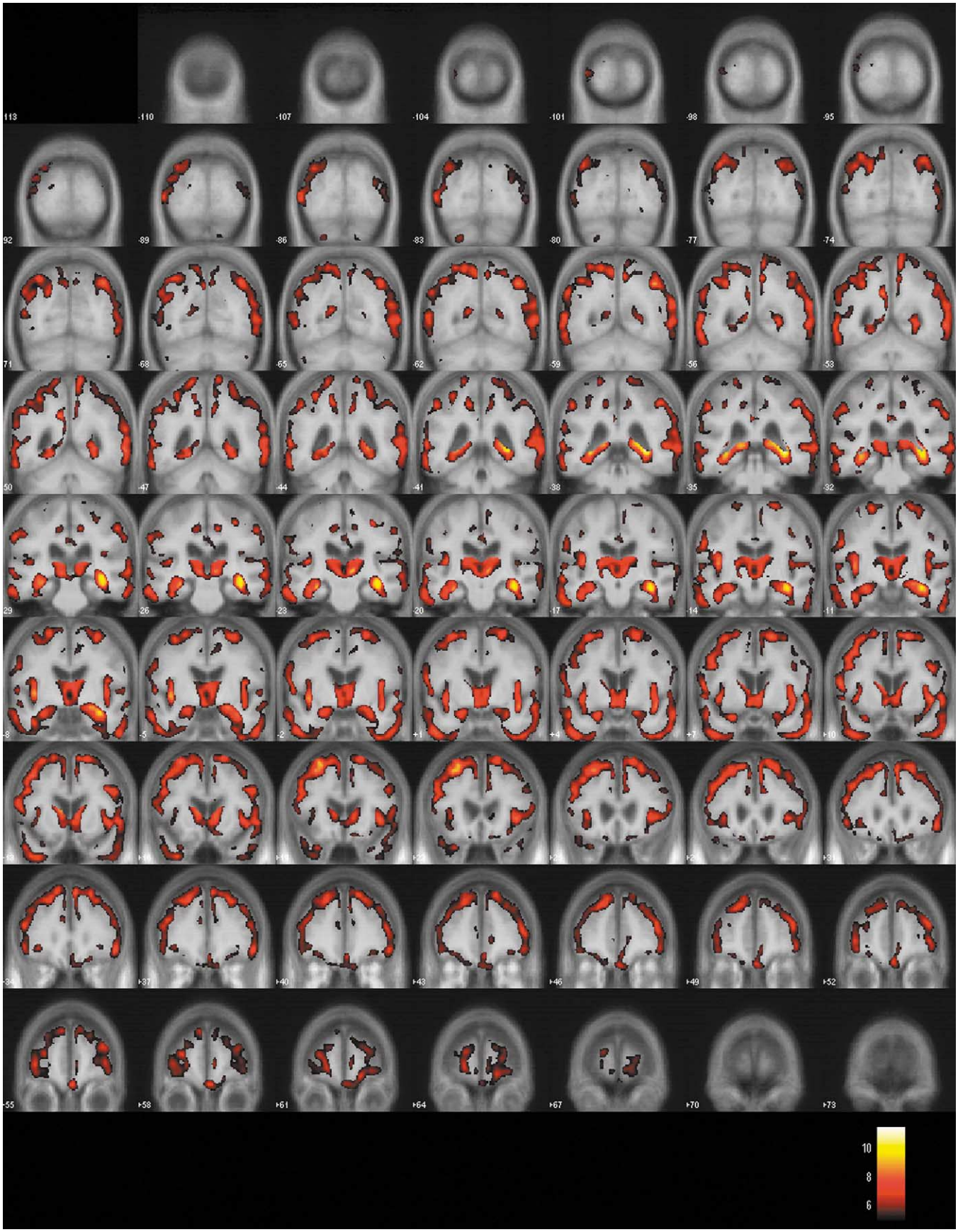

Fig. 3. Results of VBM analysis of superficial structures. The background is the local group template and the colored overlay is the contrast of gray matter being less in AD's than in controls. The color coding represents *T* values, ranging from 5.59 (dark red) to 11(yellow, almost white). A value of $T > 5.59$ corresponds to a $P < 0.05$ (corrected for multiple comparisons based on the theory of Gaussian random field). We notice diffuse cortical atrophy with asymmetric atrophy of the hippocampi bilaterally (left > right), both insulae and temporal poles. The periventricular rim has caused artifacts in the region where we expect to find the caudate and medial thalamus, so we cannot be sure if the resulting voxels are truly atrophic. More detailed analysis of these structures is described in the text (step 5) and in Fig. 4. Interestingly, sparing of the sensorimotor cortex, occipital areas, and cerebellum is evident on the series of images of the fifth row from the bottom.

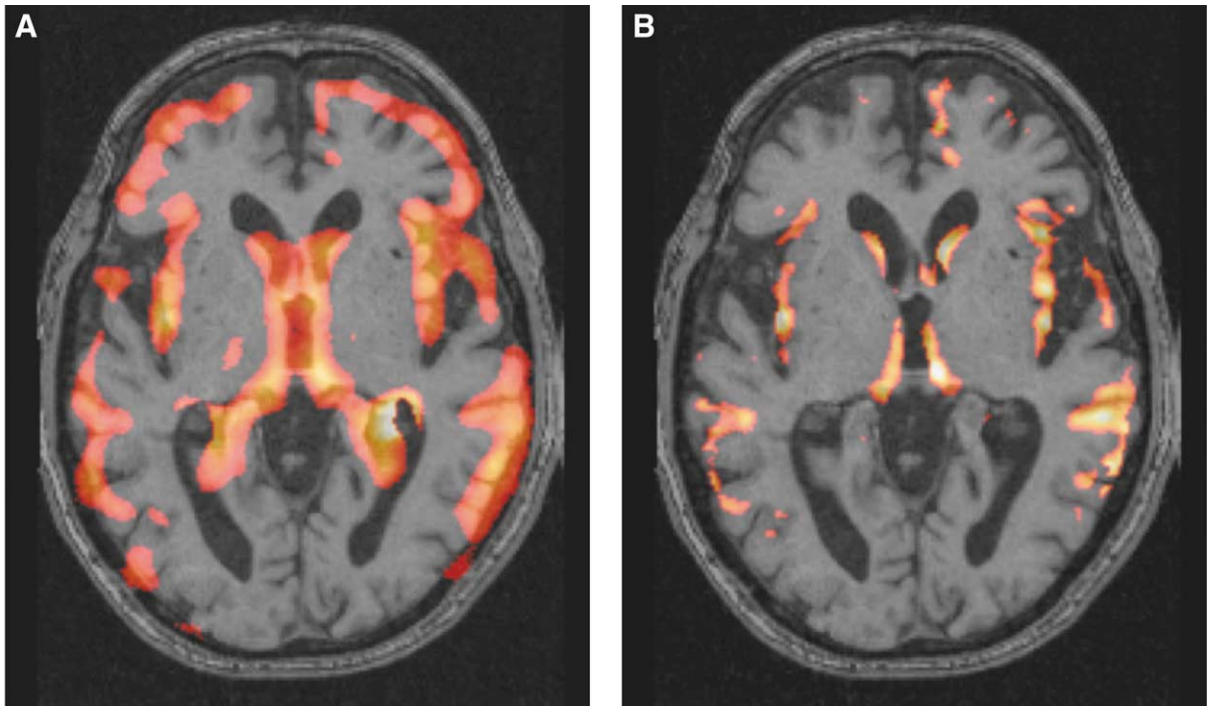

4

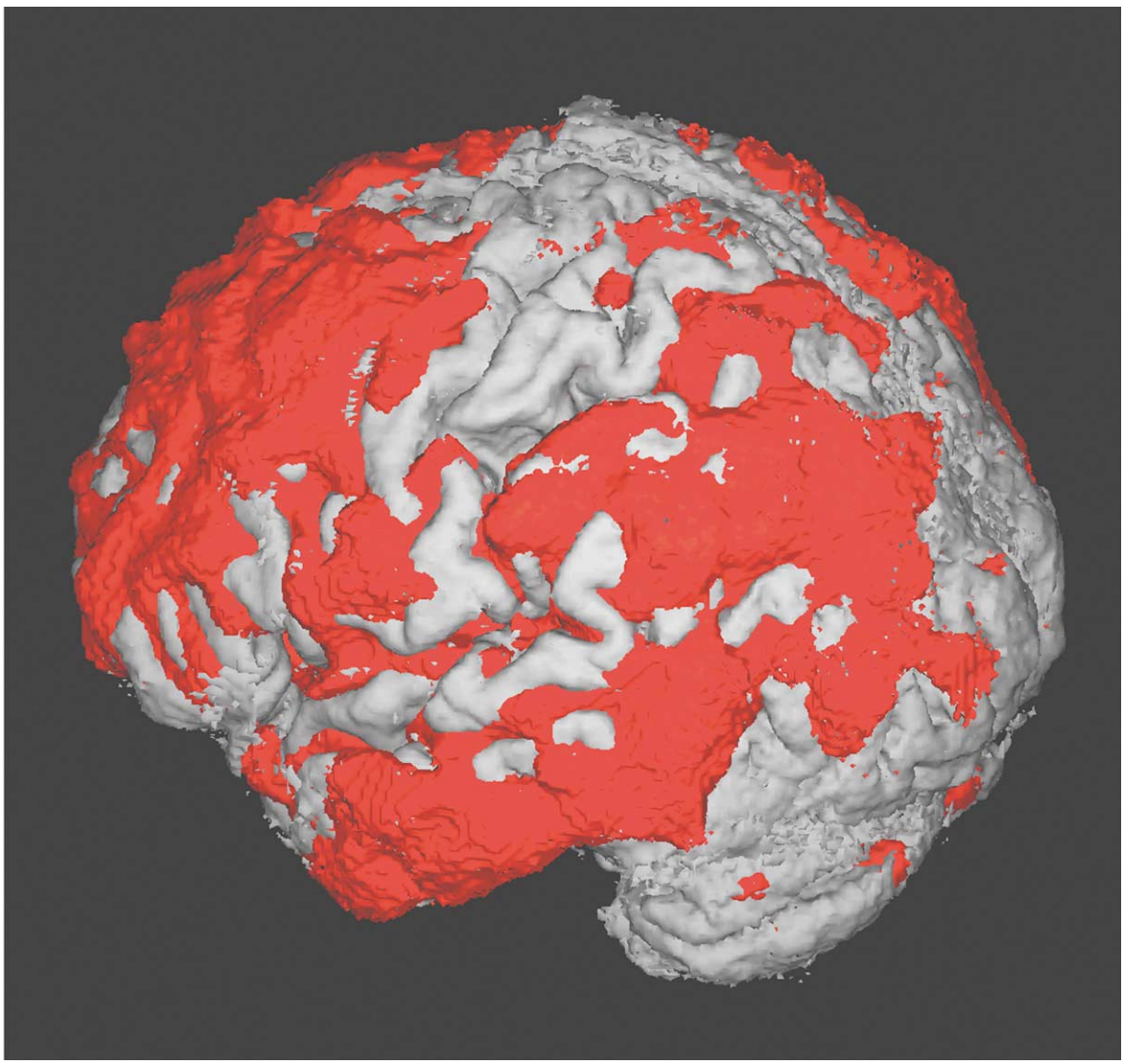

6

further analysis, during nonlinear normalization the local volumes of certain regions of the brain might expand or contract. As statistical analysis aims to identify regional differences in gray matter between groups it is important to correct for the effects of volume change. This was achieved by an additional processing step termed modulation, which multiplies the gray matter voxels by the Jacobians derived from spatial normalization and thereby preserves the amount of gray matter in each voxel (Ashburner and Friston, 2000). In essence, analysis of modulated data focuses on volume differences, while analysis of unmodulated data focuses on concentration differences. Modulation was performed on all image datasets in this study.

Erosion and dilatation

MR scans of elderly subjects tend to have larger ventricles. The voxels lying at the interface of ventricular CSF and periventricular white matter tend to assume intermediate intensities (close to gray matter) as a result of partial voluming. The Bayesian segmentation tends to misclassify these voxels as GM. This results in a thin rim of "GM voxels" around the lateral ventricular system in both the AD's and the controls. This artifact has been present in previous VBM studies of AD patients vs controls; see, for example, Fig. 1 in the VBM study by Baron et al. (2001). This poses a question about the validity of earlier findings regarding deep cerebral gray matter structures. Therefore we incorporated a morphological "opening" algorithm which is defined as gray scale erosion followed by dilatation to eliminate this thin rim of tissue (Haralick et al., 1987). The effect of morphological opening is to remove small features within the image, in our case the thin periventricular rim. The side effect of the algorithm is that thin cortical GM islands might be removed as well. This was an anticipated side effect, and that is why in the current study we used analysis of "opened" volumes to examine atrophy of deep structures, while we employ normal volumes without "opening" to evaluate cortical atrophy.

Smoothing

The spatially normalized gray matter masked images were smoothed with a 10-mm FWHM isotropic Gaussian kernel to allow for individual gyral variation and to render the data suitable for parametric statistical analysis. Our choice of a 10-mm FWHM kernel was supported by a recent publication, where it was shown that kernels between 10 and 15 mm produce higher T values for VBM (Davatzikos et al., 2001). The opened GM volumes were smoothed with a narrower kernel of 4 mm FWHM, because morphological opening results in smoothing as well (Haralick et al., 1987).

Statistical analysis

Statistical analysis used the general linear model and is based on the random Gaussian field theory (Friston et al., 1995). The design matrix for statistical analysis is composed of two contrasts comparing the smoothed gray matter. In the categorical group comparisons (AD vs Controls) voxel-by-voxel statistical differences were estimated by detecting whether each voxel has a higher or lower probability of being gray matter in the patient group than the same voxel in the control group. To normalize for global differences in voxel intensities across scans, gray matter globals were modeled as a confounding covariate in an analysis of covariance (ANCOVA) (Friston et al., 1995). By allowing for global changes, the results reflect regionally specific difference in gray matter rather than a global measure of atrophy. Differences in voxel values for each contrast form a t statistic map (SPM$\{t\}$). The SPM$\{t\}$ map is then transformed to the unit normal distribution (SPM$\{z\}$) and thresholded at $P < 0.05$ corrected for multiple comparisons at the voxel level (Friston et al., 1995). It should be noted that both positive (GM of Controls greater than of AD) and negative (GM of Controls less than of AD) contrasts were calculated.

Results

Display of results

For qualitative analysis, mean gray matter images for each group were created and visually inspected (Fig. 5). These images did not demonstrate any collateral "spreading" of gray matter structures such as the caudate nucleus and medial thalamus. For the visualization of quantitative

Fig. 4. (A) Results of VBM analysis without morphological opening and (B) after the opening operator has been applied. Results are superimposed on a single patient scan for display purposes. VBM analysis of deep structures lowers the signal of the diffuse cortical component of atrophy, but separates atrophy of the caudate and medial thalamus. This atrophy was masked by ventricular partial voluming in the initial analysis (A). The cortical component of atrophy is less prominent with this type of analysis, since thin islands of cortical gray matter are also removed. Also, highly significant voxels remain in the insular region.

Fig. 6. Three-dimensional surface rendering of a skull-stripped AD brain (gray) and AD group cortical atrophy (red) superimposed. Notice that there is diffuse cortical atrophy with sparing of the sensorimotor cortex, low occipital region, and cerebellum. Such a pattern of atrophy corresponds to neocortical stage V, as described by Braak et al. (Braak et al., 1999; Braak and Braak, 1991). It is at this stage that the initial diagnosis of AD is usually made.

Fig. 5. (A) Mean gray matter volumes (averaged) of controls' scans and (B) of AD scans. Images have been brought to intensity scale to appreciate the diffuse loss of gray matter in the AD group (darker signal). We notice what in VBM literature is commonly referred to as global vs local differences; although the approximate global size has been matched (an essential step in VBM), local differences are still visible. The locations corresponding to the average caudate nucleus and the average medial thalamus are smaller in the AD group than in the control group. We also notice increased average ventricular size in the AD group. In order to quantitate these visual differences one needs to perform statistical tests (Fig. 3). Nevertheless, there is no visible "spreading" of the aforementioned structures over a wider area. These images have not been morphologically opened and therefore we still notice the periventricular artifact.

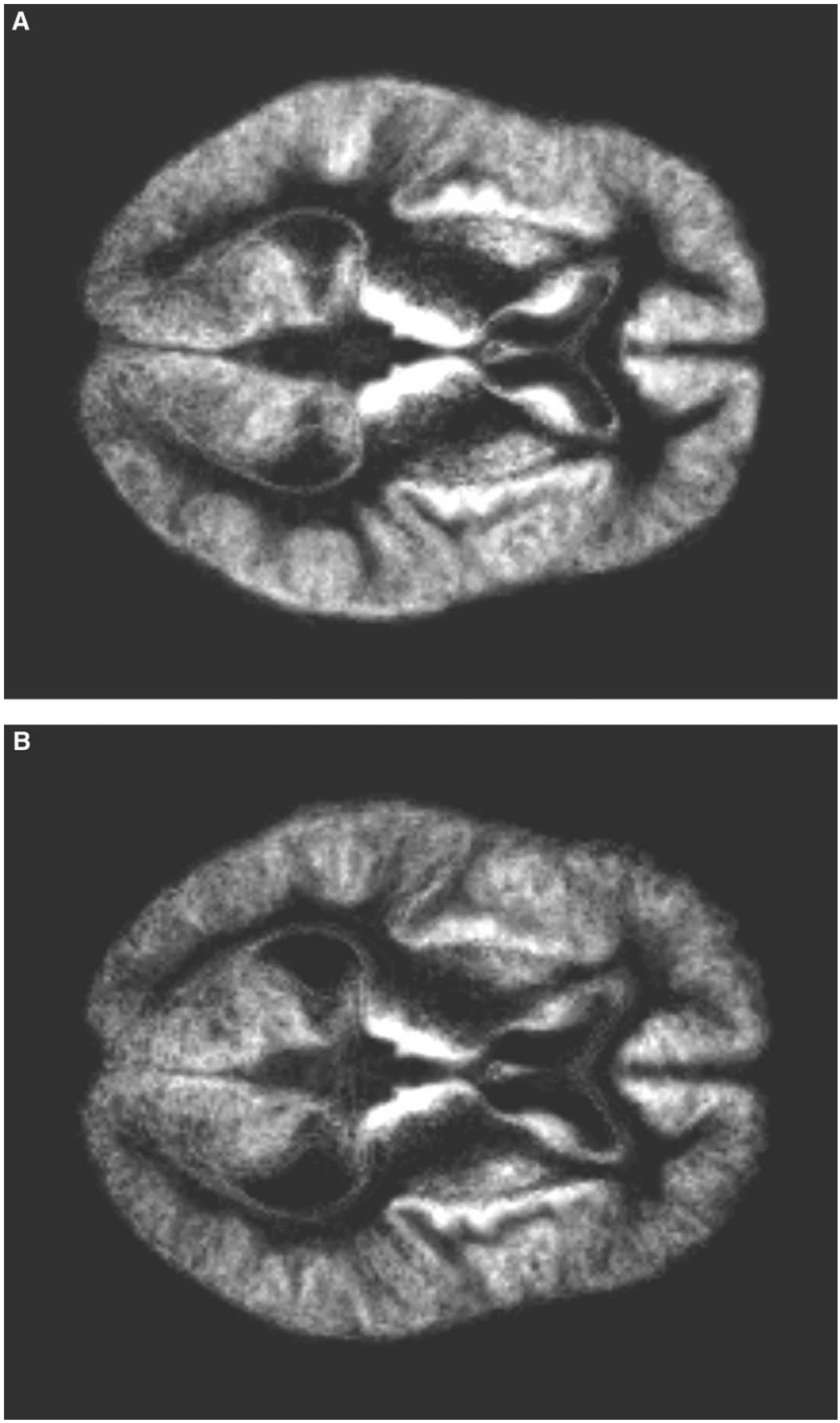
A
B

results areas of significant change were displayed in the coronal plane and overlaid on the group specific template (Fig. 3). We avoid the "glass brain" display, because we do not find it informative enough when used in a non-interactive manner, since significant regions are superimposed. The images are orientated in radiological convention (the right side of the head is on the left) and all statistical maps are displayed as a color-coded overlay, with lower *T* values having dark red color and higher values approaching the yellow side of the spectrum.

Differences in gray matter volume between AD and controls

Significant clusters of locally reduced gray matter volume were observed in AD patients relative to controls subjects. Regions of significant difference were seen to diffusely affect the cerebral cortex, with remarkable sparing of the sensorimotor cortex (Figs. 3 and 6). The gray matter surrounding the Sylvian fissure was also remarkably reduced, as well as the hippocampal and temporal pole gray matter. The occipital pole, however, was also relatively spared.

While VBM has not been developed to formally test for differences in gray matter *between* different regions in the brain (that is, between a certain region on the left and on the right), the *T* maps indicate asymmetries between hemispheres. For example, 10.3% of all MTL voxels on the left vs 7.8% of all MTL voxels on the right were above the corrected *P* value, suggesting greater left than right MTL atrophy.

As mentioned previously, the periventricular rim of false-positive gray matter produced highly significant results inside the ventricular system (smoothing of the ventricular rim spreads the false-positive voxels to a larger area). Morphological opening (step 5) resulted in removal of the thin gray matter rim, but also reduced the significance of cortical atrophy (Fig. 4). Without the periventricular artifact covering the deep gray structures, we noticed significant atrophy of the caudate nucleus and the medial thalamus. However, the putamen and globus pallidus were not affected by atrophy in any of the analyses.

Examination of the inverse contrast, i.e., gray matter loss of controls compared to AD, did not yield any significant results for any of the aforementioned analyses.

Discussion

It is well known that Alzheimer's disease is characterized by cerebral atrophy. A recent review describes the current hypotheses about atrophy patterns in AD (Smith, 2002). In the very early stages only the entorhinal cortex is affected. Later, atrophy spreads to the hippocampus proper and the MTL. Projection neurons from the MTL die, disrupting their neurotrophic support to pyramidal cells in the association areas of the cortex. Based on projections from the MTL, the cortex in the temporoparietal region is the next to be involved. Other areas of the cortex, dependent on synaptic input from the association areas, later begin to disintegrate. In late stages of the disease the entire neocortex becomes involved, with relative sparing of occipital poles and cerebellum. As pointed out by Smith "an anatomical cascade builds up" from the entorhinal cortex to involve the nearby structures first and eventually higher cortical areas (Smith, 2002).

Various studies have demonstrated several regions involved in the atrophy process, in particular the entorhinal cortex, the hippocampus, and the medial temporal lobe (de Leon et al., 2001; Frisoni, 2000). The issue not solved by these studies was that they set their focus of attention to a predefined set of structures without relating the atrophy patterns from other areas of the brain. In contrast, VBM estimates anatomical differences by considering the brain as a whole. Whereas most current ROI methods have been focusing on measurement of preselected regions, atrophy measurement and localization by VBM is performed by running millions of statistical tests between two groups (a typical structural MRI dataset has around 11 million voxels, approximately 3 million of which are brain voxels).

Our VBM implementation demonstrated in vivo diffuse cortical atrophy in AD, with the exception of the sensorimotor cortex, cerebellum, and occipital lobes. We also demonstrated atrophy of the hippocampus, insula, temporal poles, medial thalamus, and head of the caudate nucleus.

One should be cautious when using automated image processing packages for disease description and identification. Although the algorithms in SPM99 are considered robust, this software was not specifically designed for measurement of atrophy in diseased patients. Rather, it was designed for evaluation of functional MRI data and PET data. We performed the various procedures during a typical VBM session of SPM and noted certain steps, which needed to be either modified or inserted in the typical analysis (Fig. 1). As very well pointed out recently, imperfect registration can lead to inaccuracies (Bookstein, 2001). This is especially true in brain AD atrophy, where the ventricles are enlarged and registration might thus be imperfect. We attempted to tackle this problem by creating a local template, comprising both AD's and controls (Good et al., 2001b, 2001a; Toga and Thompson, 2001). When registering to a local template, AD and controls meet approximately halfway through the registration process, essentially lowering this error. Of course, anatomical variability in AD pathology and degree of ventricular expansion might mean that even with the use of a study-specific template misregistration might still occur, but would nevertheless be substantially lower than that with matching to a generic young-normal template because age effects and average AD pathology are encoded in the template. Matching of dementia scans to a disease-specific template together with measurements of goodness of match has been described in

cortical-matching studies in AD (Thompson et al., 2001). Also, with this sophisticated type of registration a similar atrophy pattern was reported, underscoring the validity of our results. A second approach is to correct for volume change, as we described in the modulation section. A third approach would be to use segmented gray matter partitions for the normalization process, a method currently under development and evaluation (Good et al., 2001b), but then use of priors for the segmentation might still be problematic.

A second step which merits attention is the segmentation procedure. One should check the histograms of the volumes to make sure no major misclassifications have taken place. Furthermore, a periventricular rim of misclassified voxels is frequently observed. This rim can be blown up because of the smoothing. One could argue that atrophy detected at the interface between gray/white matter and CSF is artificial, because that is exactly where we find strong intensity gradients (Bookstein, 2001). The argument for the strong gradients is that if a group's ventricles are enlarged, as happens in AD, then spatial normalization would shrink the surrounding structures when attempting to fit the scans to the template (Ashburner and Friston, 2001). Moreover, ventricular size variation within the AD group might have "spread" the deep gray matter structures along a wider area, thus creating the false impression of atrophy. We checked the mean GM images of the two groups, and we did not notice any spreading of the caudate nucleus or medial thalamus or any other structure over a wider area in any of the groups. Moreover, only selected structures were demonstrated; if registration had squeezed all structures, then we would have expected significant atrophy, for example, in the putamen and globus pallidus as well.

The first visual scales of AD pathology, as visualized on MRI, rate the hippocampus, insula, medial temporal lobe, and parahippocampal gyrus (Scheltens et al., 1992, 1995; Erkinjuntti et al., 1993). These scales presume that pathology in AD is concentrated in the aforementioned regions in the earliest stages of AD, a result easily identifiable with the naked eye. Our results confirmed the presence of severe atrophy in these locations, namely, the hippocampus, insula, and temporal lobe. Additionally, we also observed diffuse cortical atrophy in concordance with mild to moderate dementia severity in our sample. Cortical atrophy was not uniform; the sensorimotor cortex, occipital poles, and cerebellum were spared. Previous neuropathological publications support the notion of sensorimotor cortex sparing in the early–mid stages of AD (Braak et al., 1999; Brun and Englund, 1981; Fox et al., 2001; Samuel et al., 1991) and only one exception has been demonstrated as a case report (Golaz et al., 1992), probably reflecting a late stage in AD pathology.

There have been other cross-sectional studies examining brain atrophy without prior assumptions (Rombouts et al., 2000; Baron et al., 2001; Thompson et al., 2001). The pilot study of Rombouts et al. was the first study to report atrophy of the hippocampus, insular region, and caudate nucleus, but it failed to observe any cortical involvement. Factors which might explain the differences with our study might be that $2 \times 2 \times 2$ mm resliced scans were used compared to $1 \times 1 \times 1$ mm in the current study, a smaller group (with 8 years difference between the groups) was examined, and P values were not corrected for multiple comparisons (Rombouts et al., 2000). The group of Baron et al. reported symmetrical atrophy of the MTL, sparing of the sensorimotor cortices, occipitotemporal regions, and cerebellum, and left-sided predominance of atrophy of posterior parietal and dorsal frontal cortex. Our study reports similar findings with the addition of asymmetry in the MTL as well. It should be noted though that Baron et al. examined a group of AD patients with a higher mean MMSE score (22.4) than our AD group (mean MMSE of 15.6) (Baron et al., 2001). Moreover, in the study of Baron et al., the same downsampling as in the study of Rombouts et al. was performed: scans were resliced to $2 \times 2 \times 2$ mm, the cutoff value for multiple comparisons was set to 0.10, and no clear correction was applied for the periventricular misclassified voxels (meaning that deep gray matter results are not clear of bias). A study which used a different approach to estimate atrophy is that of Thompson et al. (2001). Although based on a different registration method, the findings of Thompson et al. are in good agreement with our data, showing diffuse neocortical pathology, with sparing of the sensorimotor cortex, occipital poles, and cerebellum. Interestingly, they emphasize left-sided predominance, which was also present in the MTL in our material.

The findings of the current study are also in agreement with the histopathological staging of Braak et al. (Braak et al., 1999; Braak and Braak, 1991). In the limbic stages severe changes in the transentorhinal and entorhinal regions and modest changes in the hippocampus, temporal poles, and insula occur (stage III), with damage expanding to neocortical association areas in stage IV. The same areas were very significantly affected on the VBM analysis (Fig. 3).

In the neocortical stages, widespread devastation of the neocortex and damage spreading from inferior temporal areas superolaterally are noted (stage V). The primary motor field, primary sensory areas, and unimodal secondary fields are still spared. This is the pattern emerging in our group of patients with clear clinical involvement.

The medial temporal lobe and neocortical alterations served as a reference point in our findings, but we also noticed other regions of atrophy. Atrophy of the caudate head and medial thalamus, as well as of the cingulum, was observed. Atrophy of the caudate has been described by neuropathological findings (Braak and Braak, 1991) and atrophy of the thalamus by MRI ROI analysis (Jernigan et al., 1991). These three structures lie geometrically in locations which are hard to evaluate with computational models. Ventricular expansion (via partial volume effects) might obscure the fact that the caudate head and thalamus might also be atrophic, whereas cingular atrophy can easily be missed and ascribed to interhemispheric fissure widening.

The method we applied, combining creation of a local affine template and morphological opening, excluded ventricular enlargement and interhemispheric widening to cause such artifacts. We can only speculate about the clinical significance of these new findings in our patient population. What is worth mentioning, though, is that these findings were present in the same group where sensorimotor sparing was documented.

Conclusion

The optimized VBM we describe here allows a comprehensive in vivo analysis of patterns of atrophy in AD, and the results are in perfect agreement with histopathological findings. In addition to hippocampal and medial temporal lobe involvement, diffuse cortical atrophy with sparing of sensorimotor cortex, occipital poles, and cerebellum was noted. Furthermore, insula, caudate head, medial thalamus, and cingulum also appeared to be involved.

Acknowledgments

G. Karas is the recipient of Grant 2001-014 from Stichting Alzheimer Nederland and S.A.R.B. Rombouts is the recipient of Grant H00.17 from Hersenstichting Nederland. Additional funds were received from the Stichting Alzheimer and Neuropsychiatry Foundation, Amsterdam.

References

Ashburner, J., Friston, K., 1997. Multimodal image coregistration and partitioning—a unified framework. Neuroimage 6, 209–217.

Ashburner, J., Friston, K., 2001. Why voxel-based morphometry should be used. Neuroimage 14, 1238–1243.

Ashburner, J., Friston, K.J., 1999. Nonlinear spatial normalization using basis functions. Hum. Brain Mapp. 7, 254–266.

Ashburner, J., Friston, K.J., 2000. Voxel-based morphometry-the methods. Neuroimage 11, 805–821.

Baron, J.C., Chetelat, G., Desgranges, B., Perchey, G., Landeau, B., de, I.S.V., Eustache, F., 2001. In vivo mapping of gray matter loss with voxel-based morphometry in mild Alzheimer's disease. Neuroimage 14, 298–309.

Bookstein, F.L., 2001. "Voxel-based morphometry" should not be used with imperfectly registered images. Neuroimage 14, 1454–1462.

Braak, E., Griffing, K., Arai, K., Bohl, J., Bratzke, H., Braak, H., 1999. Neuropathology of Alzheimer's disease: what is new since A. Alzheimer? Eur. Arch. Psychiatry Clin. Neurosci. 249 (Suppl. 3), 14–22.

Braak, H., Braak, E., 1991. Neuropathological stageing of Alzheimer-related changes. Acta Neuropathol. 82, 239–259.

Brun, A., Englund, E., 1981. Regional pattern of degeneration in Alzheimer's disease: neuronal loss and histopathological grading. Histopathology 5, 549–564.

Davatzikos, C., Genc, A., Xu, D., Resnick, S.M., 2001. Voxel-based morphometry using the RAVENS maps: methods and validation using simulated longitudinal atrophy. Neuroimage 14, 1361–1369.

de Leon, M., Bobinski, M., Convit, A., Wolf, O., Insausti, R., 2001. Usefulness of MRI measures of entorhinal cortex versus hippocampus in AD. Neurology 56, 820–821.

de Leon, M.J., Golomb, J., George, A.E., Convit, A., Tarshish, C.Y., McRae, T., De Santi, S., Smith, G., Ferris, S.H., Noz, M., 1993. The radiologic prediction of Alzheimer disease: the atrophic hippocampal formation. AJNR Am. J. Neuroradiol. 14, 897–906.

Erkinjuntti, T., Lee, D.H., Gao, F., Steenhuis, R., Eliasziw, M., Fry, R., Merskey, H., Hachinski, V.C., 1993. Temporal lobe atrophy on magnetic resonance imaging in the diagnosis of early Alzheimer's disease. Arch. Neurol. 50, 305–310.

Folstein, M.F., Folstein, S.E., McHugh, P.R., 1975. "Mini-mental state." A practical method for grading the cognitive state of patients for the clinician. J. Psychiatr. Res. 12, 189–198.

Fox, N.C., Crum, W.R., Scahill, R.I., Stevens, J.M., Janssen, J.C., Rossor, M.N., 2001. Imaging of onset and progression of Alzheimer's disease with voxel- compression mapping of serial magnetic resonance images. Lancet 358, 201–205.

Fox, N.C., Warrington, E.K., Freeborough, P.A., Hartikainen, P., Kennedy, A.M., Stevens, J.M., Rossor, M.N., 1996. Presymptomatic hippocampal atrophy in Alzheimer's disease. A longitudinal MRI study. Brain 119 (Pt. 6), 2001–2007.

Freeborough, P.A., Fox, N.C., 1997. The boundary shift integral: an accurate and robust measure of cerebral volume changes from registered repeat MRI. IEEE Trans. Med. Imaging 16, 623–629.

Freeborough, P.A., Fox, N.C., 1998. Modeling brain deformations in Alzheimer disease by fluid registration of serial 3D MR images. J. Comput. Assist. Tomogr. 22, 838–843.

Frisoni, G.B., 2000. Visual rating and volumetry of the medial temporal lobe on magnetic resonance imaging in dementia. J. Neurol. Neurosurg. Psychiatry 69, 572.

Frisoni, G.B., Beltramello, A., Weiss, C., Geroldi, C., Bianchetti, A., Trabucchi, M., 1996. Linear measures of atrophy in mild Alzheimer disease. AJNR Am. J. Neuroradiol. 17, 913–923.

Friston, K.J., Holmes, A., Poline, J.B., Price, C.J., Frith, C.D., 1996. Detecting activations in PET and fMRI: levels of inference and power. Neuroimage 4, 223–235.

Golaz, J., Bouras, C., Hof, P.R., 1992. Motor cortex involvement in presenile dementia: report of a case. J. Geriatr. Psychiatry Neurol. 5, 85–92.

Good, C.D., Johnsrude, I., Ashburner, J., Henson, R.N., Friston, K.J., Frackowiak, R.S., 2001a. Cerebral asymmetry and the effects of sex and handedness on brain structure: a voxel-based morphometric analysis of 465 normal adult human brains. Neuroimage 14, 685–700.

Good, C.D., Johnsrude, I.S., Ashburner, J., Henson, R.N., Friston, K.J., Frackowiak, R.S., 2001b. A voxel-based morphometric study of ageing in 465 normal adult human brains. Neuroimage 14, 21–36.

Gutterman, E.M., Markowitz, J.S., Lewis, B., Fillit, H., 1999. Cost of Alzheimer's disease and related dementia in managed-medicare. J. Am. Geriatr. Soc. 47, 1065–1071.

Haralick, R.M., Sternberg, S.R., Zhuang, X., 1987. Image analysis using mathematical morphology. IEEE Trans. Pattern Anal. Machine Intelligence PAMI 9 (4), 532–550.

Jack Jr., C.R., Petersen, R.C., O'Brien, P.C., Tangalos, E.G., 1992. MR-based hippocampal volumetry in the diagnosis of Alzheimer's disease. Neurology 42, 183–188.

Jernigan, T.L., Salmon, D.P., Butters, N., Hesselink, J.R., 1991. Cerebral structure on MRI, Part II: specific changes in Alzheimer's and Huntington's diseases. Biol. Psychiatry 29, 68–81.

McKhann, G., Drachman, D., Folstein, M., Katzman, R., Price, D., Stadlan, E.M., 1984. Clinical diagnosis of Alzheimer's disease: report of the NINCDS-ADRDA Work Group under the auspices of Department of Health and Human Services Task Force on Alzheimer's Disease. Neurology 34, 939–944.

Montgomery, S.M., 1979. Depressive symptoms in acute schizophrenia. Prog. Neuropsychopharmacol. 3, 429–433.

Pruessner, J.C., Li, L.M., Serles, W., Pruessner, M., Collins, D.L., Kabani, N., Lupien, S., Evans, A.C., 2000. Volumetry of hippocampus and amygdala with high-resolution MRI and three-dimensional analysis

software: minimizing the discrepancies between laboratories. Cereb. Cortex 10, 433–442.

Rombouts, S.A., Barkhof, F., Witter, M.P., Scheltens, P., 2000. Unbiased whole-brain analysis of gray matter loss in Alzheimer's disease. Neurosci. Lett. 285, 231–233.

Roth, M., Tym, E., Mountjoy, C.Q., Huppert, F.A., Hendrie, H., Verma, S., Goddard, R., 1986. CAMDEX. A standardised instrument for the diagnosis of mental disorder in the elderly with special reference to the early detection of dementia. Br. J. Psychiatry 149, 698–709.

Samuel, W.A., Henderson, V.W., Miller, C.A., 1991. Severity of dementia in Alzheimer disease and neurofibrillary tangles in multiple brain regions. Alzheimer Dis. Assoc. Disord. 5, 1–11.

Scheltens, P., Launer, L.J., Barkhof, F., Weinstein, H.C., Van Gool, W.A., 1995. Visual assessment of medial temporal lobe atrophy on magnetic resonance imaging: interobserver reliability. J. Neurol. 242, 557–560.

Scheltens, P., Leys, D., Barkhof, F., Huglo, D., Weinstein, H.C., Vermersch, P., Kuiper, M., Steinling, M., Wolters, E.C., Valk, J., 1992. Atrophy of medial temporal lobes on MRI in "probable" Alzheimer's disease and normal ageing: diagnostic value and neuropsychological correlates. J. Neurol. Neurosurg. Psychiatry 55, 967–972.

Scheltens, P., Pasquier, F., Weerts, J.G., Barkhof, F., Leys, D., 1997. Qualitative assessment of cerebral atrophy on MRI: inter- and intra-observer reproducibility in dementia and normal aging. Eur. Neurol. 37, 95–99.

Smith, A.D., 2002. Imaging the progression of Alzheimer pathology through the brain. Proc. Natl. Acad. Sci. USA 99, 4135–4137.

Smith, S.M., De Stefano, N., Jenkinson, M., Matthews, P.M., 2001. Normalized accurate measurement of longitudinal brain change. J. Comput. Assist. Tomogr. 25, 466–475.

Thompson, P.M., Mega, M.S., Woods, R.P., Zoumalan, C.I., Lindshield, C.J., Blanton, R.E., Moussai, J., Holmes, C.J., Cummings, J.L., Toga, A.W., 2001. Cortical change in Alzheimer's disease detected with a disease-specific population-based brain atlas. Cereb. Cortex 11, 1–16.

Thompson, P.M., Woods, R.P., Mega, M.S., Toga, A.W., 2000. Mathematical/computational challenges in creating deformable and probabilistic atlases of the human brain. Hum. Brain Mapp. 9, 81–92.

Toga, A.W., Thompson, P.M., 2001. The role of image registration in brain mapping. Image Vision Comput. 19, 3–24.

Trabucchi, M., 1999. An economic perspective on Alzheimer's disease. J. Geriatr. Psychiatry Neurol. 12, 29–38.

Woods, R.P., Grafton, S.T., Watson, J.D., Sicotte, N.L., Mazziotta, J.C., 1998. Automated image registration: II. Intersubject validation of linear and nonlinear models. J. Comput. Assist. Tomogr. 22, 153–165.